

Mass transfer and interfacial properties in two-phase microchannel flows

Jeffrey D Martin¹ and Steven D Hudson¹

Complex Fluids Group, Polymers Division, National Institute of Standards and Technology, 100 Bureau Dr., Gaithersburg, MD 20899-8542, USA

E-mail: jeffrey.martin@nist.gov and steven.hudson@nist.gov

New Journal of Physics **11** (2009) 115005 (26pp)

Received 1 June 2009

Published 4 November 2009

Online at <http://www.njp.org/>

doi:10.1088/1367-2630/11/11/115005

Abstract. Drop-based microfluidic devices are becoming more common, and molecular mass transfer and drop circulation are issues that often affect the performance of such devices. Moreover, interfacial properties and surfactant mass transfer rates govern emulsion behavior. Since these phenomena depend strongly on drop size, measurement methods using small drops and flow typical of applications are desired. Using mineral oil as a continuous phase, water droplets and an alcohol surfactant, we demonstrate here a microfluidic approach to measure the interrelated phenomena of dynamic interfacial tension, surfactant mass transfer and interfacial retardation that employs droplet flows in a microchannel with constrictions/expansions. Interfacial flow is influenced markedly by adsorption of surfactant: severe interfacial retardation (by a factor of 30) is observed at low surfactant concentrations and interface remobilization is observed at higher surfactant concentrations. The interfacial tension is described by Langmuir kinetics and the parameters for interfaces with mineral oil (studied here) compare closely with those previously found at air interfaces. For the conditions explored, the surfactant mass transfer is described well by a mixed kinetic-diffusion limited model, and the desorption rate coefficients are measured to be both approximately 70 s^{-1} . The transition from a diffusion-controlled to mixed diffusion-kinetic mass transfer mechanism predicted with reducing drop size is verified. This experimental approach (i.e. adjustable geometry and drop size and height) can therefore probe interfacial dynamics in simple and complex flow.

¹ Authors to whom any correspondence should be addressed.

Contents

1. Introduction, droplet-based microfluidics	2
2. Background	3
2.1. Interfacial tension, surfactant sorption dynamics and interfacial mobility	3
2.2. Mass transfer	5
3. Experimental	8
3.1. Fluids and particles	8
3.2. Pendant drop tensiometry	8
3.3. Device fabrication and design	8
3.4. Adjusting drop height	9
3.5. Microscope, pump control and data acquisition	9
3.6. Analysis of drop deformation and motion	10
3.7. Examination of flow inside drops	12
3.8. Mass transport kinetic calculations	12
4. Results and discussion	12
4.1. Analysis of drops	12
4.2. Interfacial tension versus drop age	14
4.3. Drop circulation	15
4.4. Pendant drop tensiometry and equilibrium interfacial tension	16
4.5. Applying the mixed kinetic model and comparing to experimental data	18
5. Conclusions and future directions	21
Acknowledgment	21
Appendix	21
References	23

1. Introduction, droplet-based microfluidics

Droplet-based microfluidics has emerged as an invaluable tool that facilitates unique and varied research. For example, droplet-based microfluidics can be used to create droplet flows with precise control over drop size, frequency and flow conditions (Teh *et al* 2008). This control over droplet characteristics and flow conditions has facilitated diverse experimentation. For instance, droplet-based microfluidic devices have been utilized to create double emulsion drops (Nie *et al* 2005, Utada *et al* 2005), Janus particles (Nisisako *et al* 2006), nanoliter-sized chemical reaction vessels (drops) (Ahmed *et al* 2006, Edel *et al* 2002), microcapsules for drug delivery (Kim *et al* 2007, Zhang *et al* 2006) and biologic sensors (He *et al* 2005, Sims and Allbritton 2007). A complete review of droplet-based microfluidics is beyond the scope of this work, and the interested reader is referred to a recent review on the subject (Teh *et al* 2008).

This technology presents an ideal arena to study the dynamics of emulsions because of the precise control of droplet characteristics and flow conditions. Emulsions are omnipresent in and essential to everyday life, e.g. foods, pharmaceuticals, cosmetics, paints, oil recovery, etc. The morphology and stability of such systems depend on dynamic interfacial processes and properties. Measurement of these properties and the coefficients associated with these processes is therefore fundamental and important for application. Typical methods used to measure such

properties often rely on a balance of forces that dictates drop sizes of the order of millimeters. Furthermore, these typical measurement methods often employ flows much simpler than those encountered in typical processing applications. For example, the pendant drop method relies on a balance of surface tension and gravity forces and is quiescent. This force balance requires that drops be approximately millimeters in size, whereas droplets in typical processing applications (e.g. detergents) are of the order of micrometers in size. Most importantly, the droplet size governs surfactant mass transfer mechanisms (Jin *et al* 2004). It is therefore critical that dynamic interfacial studies be conducted on droplets with sizes comparable to those found in typical applications and in appropriate flow conditions. Droplet-based microfluidics are able to address these needs. Introduction and fine-tuning of flow complexity is relatively straightforward in droplet-based microfluidic devices. Advances in the ability to create monodisperse, stable droplet flows (Anna *et al* 2003, Nisisako *et al* 2002, Thorsen *et al* 2001, Yobas *et al* 2006) and tailored, complex flow fields in microfluidic devices (Cabral and Hudson 2006, Hudson *et al* 2005) have facilitated the study of interfacial phenomena at reduced length scales and complex flows. For example, in past work a microfluidic device capable of measuring dynamic, multi-component interfacial tension was realized (Cabral and Hudson 2006, Hudson *et al* 2005).

Here, we use this microfluidic interfacial tensiometer as a means to probe interfacial dynamics and surfactant mass transfer processes at reduced length scales that are relevant in drop microfluidic and emulsion processing applications, i.e. tens of micrometers. The interfacial tension in a two-phase, surfactant-containing system is used as a direct measure of the surfactant concentration adjacent to the interface. The tension is measured dynamically and mass transfer kinetics are determined through modeling the surfactant diffusion and interfacial kinetics. Simultaneous internal circulation data using particle tracers measures Marangoni effects, i.e. interfacial immobilization. These data are combined to evaluate the rate limiting mass transfer mechanisms and to measure associated parameters. Although much experimental research has been focused on studying dynamic interfacial tension and surfactant mass transfer in two-phase systems (Ferrari *et al* 1997, Jin *et al* 2004, Liggieri *et al* 1997, Lin *et al* 1997, Miller and Kretzschmar 1991, Miller *et al* 1994, Pan *et al* 1998), a great deal of this work uses relatively large drops (millimeter-sized) in the presence of simple or no flow. Our microfluidic approach allows us to create and measure the dynamics of many drops with sizes typical of those in industrial applications. Since the drop size governs the mass transfer mechanisms, a shift from diffusion-limited to kinetic-limited (interfacial adsorption/desorption) mass transfer is expected (Jin *et al* 2004). Furthermore, droplets can be subjected to easily tunable complex flows, component concentrations can be easily changed through manipulation of inlet flows, and the total volume of experimental material needed is very small. Most importantly, our approach gives us the unique ability to perform high-throughput measurements of interfacial tension, surfactant mass transfer kinetics and Marangoni effects in a single experiment.

2. Background

2.1. Interfacial tension, surfactant sorption dynamics and interfacial mobility

In two-phase systems with surface-active solutes, many techniques have been employed to measure the interfacial tension as a function of time. For example, bubble pressure tensiometry utilizes measurements of the capillary pressure of bubbles forced out of a capillary to determine the interfacial tension. This technique can be employed to study dynamic interfacial tensions

from the sub-millisecond range to times of the order of tens of seconds (Fainerman and Miller 1995, Fainerman *et al* 2004, 2006, Passerone *et al* 1991). Other common methods of measuring dynamic interfacial tension include sessile and pendant drop methods, whose dynamic range is from a few seconds to a very long time (Lin *et al* 1990, Miller and Kretzschmar 1991). Although our microfluidic technique has limited time range (here 0.5–20 s), it has a number of other features advantageous for emulsion characterization, which will be discussed in this section.

Because of the balance of forces involved, the common methods (of bubble pressure and pendant drop tensiometry) must employ droplets with sizes of the order of millimeters or larger. As mentioned previously, many typical applications have drop sizes less than 100 μm . Recent studies have shown that when considering surfactant-containing two-phase systems with micrometer-sized drops, the size of the droplet is important in determining the governing mass transfer mechanisms (e.g. diffusion limited versus interfacially limited kinetics) (Jin *et al* 2004). More specifically, Jin *et al* assuming Langmuir kinetics and a planar interface, define an intrinsic length scale given by

$$R_{D-K} = \frac{D}{\beta\Gamma_{\max}}, \quad (1)$$

where D is the surfactant diffusion coefficient, β is the interfacial adsorption kinetic constant, and Γ_{\max} is the interfacial concentration corresponding to maximum packing of surfactant. Jin *et al* state that mass transfer is diffusion-controlled when the droplet radius $a \gg R_{D-K}$ and kinetically controlled when $a \ll R_{D-K}$. Nevertheless diffusion often remains important when $a \ll R_{D-K}$, since diffusion and sorption processes are in series. When this is the case, the limiting mechanism of mass transport is mixed (kinetic and diffusion). The value of R_{D-K} depends on the properties of the surfactant/two-phase system, and typical values were found to be of the order of tens of microns (Jin *et al* 2004). Alvarez *et al* have recently recalculated R_{D-K} for a spherical geometry (when curvature of the interface is important), and found R_{D-K} to be somewhat larger than given in equation (1) (Alvarez *et al* 2009). For local equilibration near a planar interface, molecules are displaced from a depth $\delta = \Gamma/c_0$ near the interface, where c_0 is the initial bulk surfactant concentration. In our experiments, as noted below, the surfactant concentration is sufficiently high that δ is very small, approximately 10 to 80 nm, and the planar interface approximation is appropriate. R_{D-K} (equation (1)) is thus predicted to be approximately [80, 200] μm for our system, depending on surfactant concentration. Our microfluidic approach allows generation of droplets with diameters of the order of tens of micrometers, facilitating experimentation at droplet length scales smaller than R_{D-K} . At these length scales, the transition from diffusion-controlled to mixed kinetically controlled surfactant mass transfer can be verified.

Beyond the ability to measure dynamic interfacial tension on droplets with diameters of the order of tens of micrometers, our microfluidic approach has the advantage of facilitating the study of drops in complex flow conditions like that which emulsions encounter in many industrial processes. This is accomplished by introducing flow complexity through variation of the microchannel geometry (see the appendix). Interfacial dynamics have typically been studied in simple, symmetric flows and it is unknown if the breaking of symmetry influences dynamics. Typical processing applications involve complex flows and different symmetries and it is unknown if interfacial dynamics in complex flows are perhaps just a superposition of simpler effects.

When studying surfactant-containing drops under flow, one must consider that the flow can convect surfactant adsorbed on the interface and interfacial surfactant concentration gradients can arise. These concentration gradients can in turn induce Marangoni effects, which retard the interface and lead to interfacial immobilization (Milliken and Leal 1994, Milliken *et al* 1993, Pawar and Stebe 1996, Stebe *et al* 1991, Stone and Leal 1990). Generally, interfacial immobilization through Marangoni effects is maximized when the quantity $\partial\sigma/\partial\Gamma$, where σ is the interfacial tension and Γ is the interfacial surfactant concentration, is large and when surface diffusion and surfactant exchange to and from the interface are slow. (Physically, the quantity $\partial\sigma/\partial\Gamma$ is a measure of the ability of a surfactant to change the interfacial tension through a change in interfacial concentration.) This interfacial immobilization arrests internal droplet fluid motion. Our microfluidic approach allows us to image drops under flow and, by placing particle tracers inside the drops, directly measure interfacial immobilization caused by Marangoni effects.

2.2. Mass transfer

The increased surface-to-volume ratio that arises in microfluidic applications can have significant effects on mass transfer. In general, flows encountered in microfluidic devices are typically laminar, and as a result, mass transfer between phases typically occurs primarily through diffusion (convection can become important in droplet/slug systems). However, this limitation is somewhat mitigated by the fact that mass transfer occurs over small length scales inherent in microfluidic devices.

Mass transfer between phases in microfluidics have been studied for a number of systems including exchange to and from droplets and slugs (Dessimoz *et al* 2008), and counter-flow (Kang *et al* 2008) and co-flow schemes (Benninger *et al* 2007, Berthier *et al* 2009, Matthews *et al* 2007, Ristenpart *et al* 2008, Salmon *et al* 2005, Sato *et al* 2003, Tokeshi *et al* 2002). In co-flow devices, two streams, miscible or immiscible, are brought into contact and flow side by side down a channel, with mass transfer between the streams occurring by diffusion (Kamholz and Yager 2001, Kamholz *et al* 1999, 2001); whereas in counter-flow devices, two streams flow toward each other in a channel, meet and exit through channels perpendicular to the initial flow direction. In the case of droplets and slugs, mass transfer occurs between the continuous phase and droplets or slugs as they flow through the channel (Burns and Ramshaw 2001, Kumemura and Korenaga 2006, Mary *et al* 2008). Most of the aforementioned work utilizing co-flow and counter-flow schemes involves single-species diffusion from one stream or phase into a second stream or phase, with a chemical reaction taking place in the initially solute-free stream or phase. Typically, some optical parameter of the fluid changes as the reaction proceeds, allowing for measurement of solute diffusion and reaction rate constants (Baroud *et al* 2003). For immiscible phases, interfacial mobility and kinetics and their effect on microfluidic mass transfer processes needs further study.

In the experiments reported here, aqueous droplet flows in mineral oil are created, and a surfactant begins only in the drop and escapes into the surrounding medium. Since the concentrations of surfactant adjacent to the interface are quasi-equilibrated by kinetic interfacial sorption processes (equations (5) and (13)), the interfacial tension measured at a given droplet or interface age is a direct measure of these local surfactant concentrations. Thus by measuring interfacial tension, the local surfactant concentration can be inferred.

At larger length scales, surfactant transport occurs through diffusion and convection, with the relative importance of each depending on experimental conditions. For diffusion, the appropriate timescale is Dt/a^2 , where t is time, while for convection it is ut/a , with the relevant velocity, u , differing for convection inside and outside the drop whose radius is a . When considering convection outside the drop, the appropriate velocity is the velocity of the drop u_d itself moving relative to the fixed channel. For convection inside the drop, the appropriate velocity is the velocity of the drop relative to that of the adjacent streamlines, which when the drop is on the centerline is approximately $u_d(2a/h)^2$, where h is the channel height. For a drop off of the centerline, the relative velocity of the adjacent streamlines can be calculated similarly. We note that even when convection is rapid, diffusion remains essential if the flow is laminar and non-chaotic. Chaotic flow inside drops may occur (Stone *et al* 1991), even in simple circumstances when translational and simple shear flows are superposed (Bryden and Brenner 1999), e.g. when a droplet rises or falls while moving in a microchannel. However, it has been shown that symmetric flows, e.g. Poiseuille, possess invariants (functions constant along streamlines) which are a barrier to convective transport inside droplets (Grigoriev 2005, Grigoriev *et al* 2006), so that transport across these streamlines remains diffusion limited. We will consider cases when the flow is non-chaotic both inside and outside of the drop. Let us now consider the internal circulation in more detail.

The flow fields inside and outside of nearly spherical drops have been determined for simple shear and extensional flow by Taylor (Taylor 1932, 1934). The flow fields for nonlinear flow were calculated by Hetsroni and Haber (1970) and expressed in simplest terms by Nadim and Stone (1991). In a drop on the channel centerline in Poiseuille flow, the scaling of the internal circulation velocity at the midplane of the drop relative to its frame of reference is given by

$$\hat{u} = \frac{u_c/u_d}{(2a/h)^2}, \quad (2)$$

where u_c is the circulation velocity inside the droplet at a point of interest. In this paper, we consider \hat{u} only at the center of the drop. In wide rectangular channels, \hat{u} there ranges from 0 to 0.5 depending on drop viscosity and interfacial retardation (Nadim and Stone 1991). (When the aspect ratio of the channel cross section w/h decreases, \hat{u} increases, e.g. $\hat{u} \cong 0.85$ when the aspect ratio is unity). In our experiments, the relative viscosity of the drop is nearly zero (giving maximum \hat{u}), but the interfacial retardation is variable depending on fluid formulation. For example, Marangoni effects caused by surfactants reduce \hat{u} through interfacial immobilization.

As mentioned above, surfactant transport occurs through diffusion and convection. Let us consider four limits: firstly, when convection is negligible; secondly, where convection inside the drop is slow, but fast outside the drop; thirdly, when convection inside and out are fast; and fourthly, when the kinetics at the interface become a limiting factor.

Firstly, when convection is negligible, the diffusion problem has been described by Liggieri *et al* (Ferrari *et al* 1997, Liggieri *et al* 1997), an extension of Ward and Tordai's analysis (Ward and Tordai 1946). When diffusion limited and with no partitioning across the interface, the concentration of surfactant is given as a function of radius r and time t by the equation

$$\frac{c}{c_0} = \frac{1}{2} \left(\operatorname{erf} \left(\frac{a-r}{2\sqrt{Dt}} \right) + \operatorname{erf} \left(\frac{a+r}{2\sqrt{Dt}} \right) \right) - \frac{\sqrt{Dt/\pi}}{r} \left(\exp \left(\frac{-(a-r)^2}{4Dt} \right) - \exp \left(\frac{-(a+r)^2}{4Dt} \right) \right). \quad (3)$$

When surfactant transport from a sphere is rate limited by diffusion, almost all (92%) of the surfactant is lost by the characteristic time a^2/D . The time to lose 50% of the surfactant is approximately one-fifth of this, which in the experiments here is somewhat less than 1 s.

Next, let us consider slow convection inside the drop, and fast outside the drop. The external Peclet number is given by $Pe_{\text{ext}} = au_d/D$, which in our experiments is $O(100)$. Since the flow is laminar ($Re = O(0.1)$), it convects components only along, and not transverse to, the channel. Thus, if the drops are very far apart, then the external convection, i.e. shear dispersion, would be significant. In such a case, the dilution effect is complicated. However, in our experiments the drops follow relatively closely in one another's wakes, and thus dilution is essentially diffusion controlled. Typically, the ratio of the distance between drops to the drop radius x_s/a is between 6 and 10. The ratio of the time it takes for a surfactant molecule to diffuse a distance equal to the drop radius a to the time it takes for a drop in the train to translate a distance of x_s is therefore $u_d a^2/x_s D$. At the experimental conditions studied here, this ratio $u_d a^2/x_s D = [20, 50]$. Therefore, except for very short times, external convection and external shear dispersion have a weak effect on dilution, and diffusive mass transfer transverse to the streamlines is dominant, and thus this case is essentially like the first.

When the convection inside and outside the drop are fast, the fountain flow inside the drop constantly brings solute from the droplet center to near the interface. (In linear shear, the streamlines in the drop are more or less parallel to the interface, and thus not effective for transport from the center.) The internal Peclet number of the fountain flow is given by

$$Pe_{\text{int}} = 4a^3 \hat{u} u_d / h^2 D = Pe_{\text{ext}} \hat{u} (2a/h)^2. \quad (4)$$

When Pe_{int} is more than unity, the mass transport at short times is significantly accelerated in comparison to the first two cases (Carslaw and Jaeger 1959, Shraiman 1987). Since this is analogous to increased diffusivity, the size R_{D-K} (equation (1)) effectively increases.

As mentioned above in section 2.1, when diffusion is fast compared to the surfactant adsorption/desorption kinetics at the interface, its mass transfer becomes limited by the kinetics at the interface. Because the drop size in our system $a_0 = [30, 50] \mu\text{m}$ is less than but still somewhat comparable to R_{D-K} , a mixed diffusion-kinetic model is appropriate (Miller and Kretzschmar 1991). According to the Langmuir model, the interfacial sorption kinetics are governed by the following equation:

$$\frac{d\Gamma}{dt} = \beta_w c_w (\Gamma_{\text{max}} - \Gamma) - \alpha_w \Gamma + \beta_{\text{oil}} c_{\text{oil}} (\Gamma_{\text{max}} - \Gamma) - \alpha_{\text{oil}} \Gamma, \quad (5)$$

where α_i are the surfactant interfacial desorption kinetic constants and c_i are the concentrations adjacent to the interface. $c_i^* = \alpha_i/\beta_i$ are characteristic concentrations (noted below) that measure interfacial activity. The characteristic time for desorption from the interface is proportional to $1/\alpha_i$, as appropriate, independent of drop size.

In summary, mass transport may be mixed mode or limited by either interfacial kinetics or diffusion, depending on the magnitude of the droplet radius a with respect to R_{D-K} (equation (1)). In addition, convection inside the drop may accelerate bulk transport there if Pe_{int} is substantial, increasing the effective size of R_{D-K} , and causing interfacial kinetics to play a greater role.

3. Experimental

3.1. Fluids and particles

Fluids used in this study are mineral oil (white, heavy, Aldrich)², n-butanol (Mallinckrodt) and distilled water. Aqueous solutions of n-butanol of (0.20, 0.50, 1.0, 2.0 and 5.0)% mass fraction were prepared. A small amount (less than 0.2% mass fraction) of polystyrene (PS) spheres (diameter $2.092 \pm 0.095 \mu\text{m}$, Polybead, Polysciences, Inc.) were placed into the aqueous drops to serve as particle tracers. The mineral oil, n-butanol and PS spheres were used as received. The viscosity of the mineral oil is 0.17 Pa s at 22°C .

3.2. Pendant drop tensiometry

Interfacial tension was measured by pendant drop tensiometry (ITConcepts, France), using a 20 gauge needle. The pixel dimensions in each direction were calibrated (Yeh and Chen 2001) to give an air water surface tension of 72.0 mN m^{-1} at 25°C , independent of drop size (surface area ranging from 7 to 30 mm^2). Thus calibrated, the interfacial tension between the heavy mineral oil and water was also independent of drop size and found to be $52 \pm 1.5 \text{ mN m}^{-1}$ at 22°C . The interfacial tension was measured as a function of time from several seconds to several days, as discussed in section 4.4.

3.3. Device fabrication and design

Fabrication of the microfluidic device from soft lithography and polydimethylsiloxane (PDMS, Dow Sylgard) replication has been described in detail previously (Cabral and Hudson 2006, Duffy *et al* 1998, Whitesides *et al* 2001). Briefly, a master channel pattern was fabricated on a Si wafer using SU-8, 2075 photoresist (MicroChem) and traditional photolithographic techniques. A PDMS device is created from the pattern, bonded to a glass slide by briefly exposing both to O_2 plasma, then fitted with tubing. Aqueous drops are formed at a T-junction and travel into the main channel which contains multiple constrictions/expansions. The droplet formation zone and a detailed geometry of constrictions/expansions can be seen in figures 1 and 3. Three inlets are provided for the continuous fluid (two leading directly into the main channel, numbers one and two, and one for drop formation, number three in figure 1) so that the drop formation rate, spacing, size and overall flow rate can be easily adjusted. Multiple inlets are also provided for the aqueous phase (numbers four and five) so that the surfactant and tracer particle concentrations can be controlled. (The circular zones in channels 3, 4 and 5 are strictly for stability of the SU-8 master.) Total flow rates, q_{tot} , were dependant on the desired size, frequency and velocity of the drops; typical operating values were between 2 and 3.5 mL h^{-1} . Multiple constrictions/expansions at various positions along the channel allow for probing of dynamics at varying drop ages. There are slight variations in channel height h throughout the channel, with the average height being $270 \pm 19 \mu\text{m}$. All other device dimensions can be inferred from figure 1.

² Certain commercial materials and equipment are identified in this paper in order to adequately specify the experimental procedure. In no case does such identification imply recommendation or endorsement by the National Institute of Standards and Technology, nor does it imply that these are necessarily the best available for the purpose.

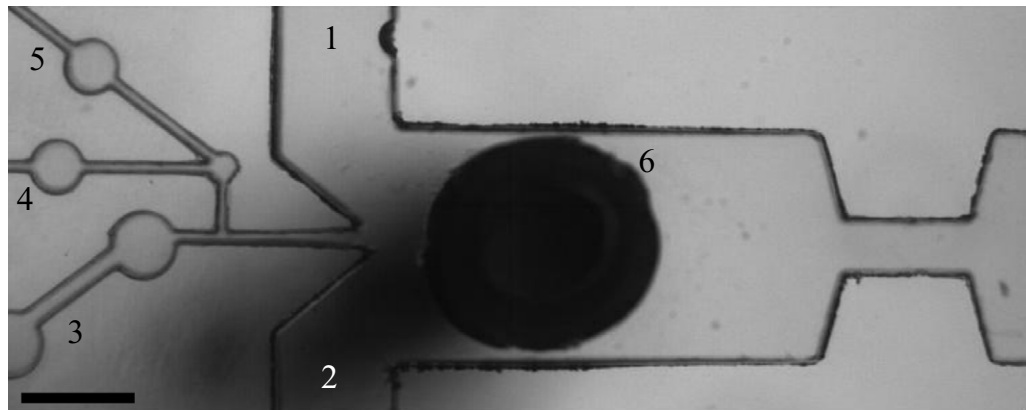


Figure 1. Optical micrograph showing droplet mixing zone, formation zone, inlet for controlling droplet height (dark circle) and a constriction (at right). Scale bar represents $500\ \mu\text{m}$.

3.4. Adjusting drop height

As mentioned previously, an advantage of our device is that the flow kinematics can be easily adjusted by means of channel geometry, drop size and drop height. Unfortunately, because of small variations in geometry during fabrication, each device forms droplets at different vertical heights. Therefore, it is advantageous to be able to exert precise control over the droplet height. The droplet height, y' , is given by

$$y' = \frac{y}{h} - 0.5, \quad (6)$$

where y is the actual height of the drop in the channel. y' is measured by first focusing the microscope on the channel floor and ceiling, then the drop midplane, and noting the distances travelled by the objective. Precise control of the droplet height y' is achieved easily (see figure 2) through the injection or withdrawal of the continuous fluid through a sixth inlet (flow rate q_6) positioned above the main channel directly downstream of the droplet formation zone (see dark circle in figure 1). Continuous phase fluid is pumped either into or out of the channel to raise or lower the drop to the desired height, which in this study is the midplane of the channel. At this height, the flow in the wide channel (between constrictions) is mainly quadratic. Since this quadratic flow is relatively weak, it is overwhelmed and the flow is primarily planar extension upon entry to and exit from the constriction (other flow kinematics may also be obtained as discussed in the appendix). The inlet q_6 allows for precise control of droplet height over a wide range of y' , which facilitates precise control of flow complexity (see the appendix). The uncertainties shown in figure 2, and all figures, are standard uncertainties.

3.5. Microscope, pump control and data acquisition

Microfluidic devices are mounted on an automated translating XY stage (Prior H107) fitted on an Olympus IX71 inverted microscope. Inlets are connected to micro-stepping syringe pumps (New Era) capable of delivering fluid volumes with accuracy better than 0.1% (with known syringe diameters). The pumps and data acquisition scheme are computer-controlled though a LabVIEW routine. Eight-bit grayscale images (1504×400 pixels) are acquired with a

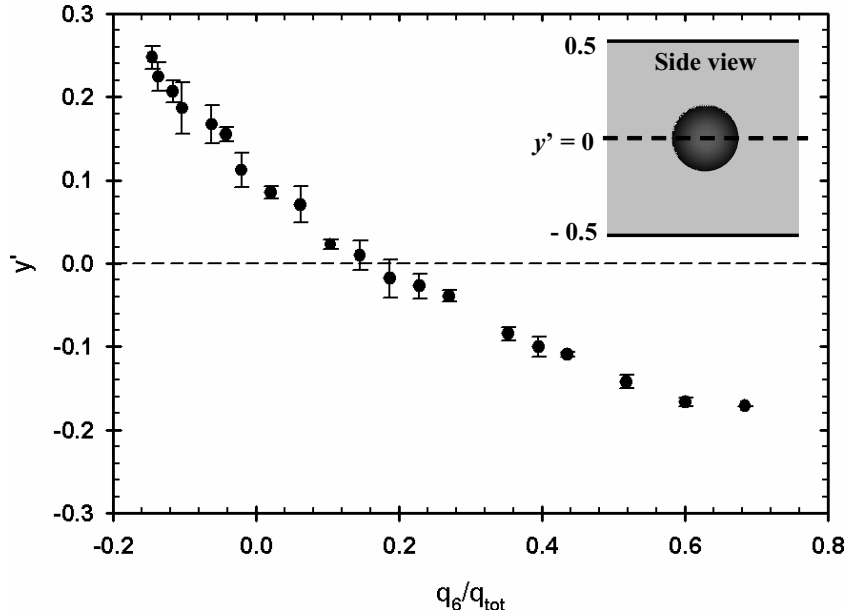


Figure 2. The dimensionless drop height versus relative flow rate into or out of the sixth inlet (see text and figure 1). Schematic of non-dimensional drop height is shown in insert.

Redlake HG-100K high-speed camera at 1000 Hz. To avoid blurring, exposure times are chosen (typically 20–50 μ s) so that the motion of the droplets is less than one pixel per exposure. Image analysis allows recording of instantaneous drop center of mass, deformation, orientation and detailed shape with time.

3.6. Analysis of drop deformation and motion

As described previously (Cabral and Hudson 2006, Gonzalez-Mancera 2007, Hudson *et al* 2005, Rallison 1984, Taylor 1932, 1934), the interfacial tension can be determined by plotting the transient response of an isolated drop to deformation in an unbounded extensional flow field (Taylor analysis):

$$\kappa \eta_c \left(5 \frac{\dot{\epsilon}_1 - \dot{\epsilon}_2}{4\hat{\eta} + 6} - \frac{d\mathcal{D}}{dt} \right) = \sigma \frac{\mathcal{D}}{a_0} \quad (7)$$

where the viscosity ratio $\hat{\eta} = \eta_d/\eta_c$, and η_d and η_c denote the droplet and continuous phase viscosities, respectively. $\dot{\epsilon}_i$ denotes a principal extension rate, a_0 is the undeformed drop radius, and \mathcal{D} is the deformation, given by

$$\mathcal{D} = \frac{L - B}{L + B}, \quad (8)$$

where L and B are the major and minor axes of the droplet, respectively. The term $\kappa \eta_c$ is an ‘effective viscosity’, where κ is a function of viscosity ratio given by the equation

$$\kappa = \frac{(2\hat{\eta} + 3)(19\hat{\eta} + 16)}{40(\hat{\eta} + 1)}. \quad (9)$$

It is important to note that for rapidly accelerating flows (entrance or exit to a constriction), the material rate of change of the extension rate becomes non-negligible and the instantaneous droplet deformation lags the steady state deformation. Equation (7) takes into account this effect.

During data acquisition, the Taylor analysis is applied in the following manner. First, a threshold is applied to the raw image resulting in a binary image, from which the droplets are extracted. The transit time of the drops $t(x)$ (x is the droplet center of mass) and the deformation \mathcal{D} are computed from the binary images. The deformation \mathcal{D} is calculated from the moments of inertia of the drops rather than directly measuring the major and minor drop axes. Calculating \mathcal{D} in this manner is a more accurate description of the droplet deformation in our system and has virtually no effect on the computation time. The transit time and deformation are then fit to polynomials (generally, the fit is insensitive to polynomial order above 5), and the extension rate along the x -direction is calculated by

$$\dot{\epsilon} = \frac{du_d}{dx} = - \left(\frac{dt}{dx} \right)^{-2} \frac{d^2t}{dx^2}, \quad (10)$$

where t is the time since the droplet entered the frame, and u_d is the droplet velocity dx/dt (the droplet is a marker of the flow). $\partial \mathcal{D} / \partial x$ is computed from the data, and the material time derivative of \mathcal{D} is calculated by the equation

$$\frac{d\mathcal{D}}{dt} = u_d \frac{\partial \mathcal{D}}{\partial x}, \quad (11)$$

which is true for unidirectional, time-invariant flow. Knowing the component viscosities, a plot of the left-hand side of equation (7) versus \mathcal{D}/a_0 is made and the slope of this plot yields the interfacial tension σ .

Because we are working with surfactant-containing systems, we must keep in mind that deviations from ideal behavior (non-spherical and non-ellipsoidal shapes) can occur. Depending on various properties of the surfactant, its concentration, the droplet history, and the external and internal flow fields, gradients in surfactant concentration along the interface can develop. These gradients can lead to deviations from ideal behavior, e.g. deviations from ideal shapes and partial or full immobilization of the interface (Gonzalez-Mancera 2007, Hu and Lips 2003, Milliken and Leal 1994, Milliken *et al* 1993, Pawar and Stebe 1996, Stone and Leal 1990, Stebe *et al* 1991). An ellipsoidal droplet shape is assumed in the determination of the interfacial tension; therefore, non-ellipsoidal shapes can introduce errors in σ . However, these non-ideal effects are expected to be minimized at small deformations where the Taylor analysis is applicable. A comprehensive discussion on other sources of error (e.g. focus, threshold and confinement) in the determination of σ through droplet deformation has been given previously (Cabral and Hudson 2006, Gonzalez-Mancera 2007).

The ability to directly measure the aforementioned non-ideal surfactant effects is one of the primary goals of this paper (e.g. measurement of interfacial immobilization through internal circulation velocity). Therefore, it would also be advantageous to be able to precisely measure non-ideal droplet shapes by determining the position of the droplet interface to a high precision (sub-pixel resolution). A detailed shape analysis routine capable of such measurements was written and incorporated into the LabVIEW primary control and analysis program. This shape analysis was not incorporated into the current study, but will be utilized in future studies.

3.7. Examination of flow inside drops

Flow fields inside of the droplets are visualized by the motion of the PS particle tracers. A series of images (focused on the droplet mid-plane) are saved and each drop is extracted from each image, yielding a single series of (smaller) images in the reference frame of the drop for each drop passing through the channel. To quantify the circulation in the droplet, we have chosen to use the velocity in the center of the droplet, given by equation (2) and illustrated schematically in figure 5. The circulation velocity u_c is calculated by tracking the position of a particle x_p near the drop center as it moves a distance comparable to the droplet radius, and fitting x_p versus t . At a frame rate of 1000 Hz and for a droplet in the channel, a particle on the centerline typically travels a distance comparable to the droplet radius over a period of about 200 images.

3.8. Mass transport kinetic calculations

The mixed diffusion-kinetic model was modeled with a one-dimensional finite element model (COMSOL 3.2, COMSOL AB). For convenience, we followed the one-dimensional mapping of Liggieri *et al* (1997). Parameters in the model include the drop size (determined experimentally), butanol diffusivity in water and oil (assumed to be $9.5 \times 10^{-10} \text{ m}^2 \text{ s}^{-1}$ in each phase (Li and Ong 1990)), and coefficients of equation (5) (Γ_{max} and c_1^* were determined by pendant drop tensiometry). Diffusion limited predictions were simulated artificially by either increasing the rate constants sufficiently, or reducing D and rescaling t accordingly.

4. Results and discussion

4.1. Analysis of drops

The fundamental basis of this investigation is particle and drop tracking. Quantities derived from these primary measurements of particle position, and drop position and shape (sample data are shown in figure 3) are the drop velocity, the rate of strain in the continuous fluid, the interface age, the internal circulation rate and the interfacial tension, as described in the previous section. As also noted in section 3.4, the drop height is adjusted to the centerline, and the drop velocity matches well the predicted centerline velocity u_{max} of a rectangular channel (figure 3) (Chatwin and Sullivan 1982)

$$u_{\text{max}} = \frac{3}{2} \frac{q_{\text{tot}}}{wh} \left(1 - 0.630 \frac{h}{w} \right)^{-1}. \quad (12)$$

This velocity is plotted in figure 3 for the sections of the channel that are of constant cross section (w, h) or (w_c, h). The slip velocity of the drop (difference from u_{max}) is expected to be small ($O(1\%)$) since the drop is relatively small (Chan and Leal 1979, Hiller and Kowalewski 1987).

The interface age is the drop passage time to travel a distance x , approximately $t_{\text{passage}} = \int_0^x dx/u_d$, which for constant flow velocity u_o is simply x/u_o . Integrating the curve in figure 3, we find for this device that $t_{\text{passage}} \cong \frac{x-1.38n}{u_o}$, where x and u_o are expressed in mm and mm s^{-1} , respectively, and n is the number of constrictions passed. Droplet residence times ranging from approximately 0.5–20 s can be realized using our current experimental setup.

As mentioned previously, the circulation of fluid inside the drop is measured by tracking the tracer particles in the drop. This circulation is noteworthy because it directly probes the

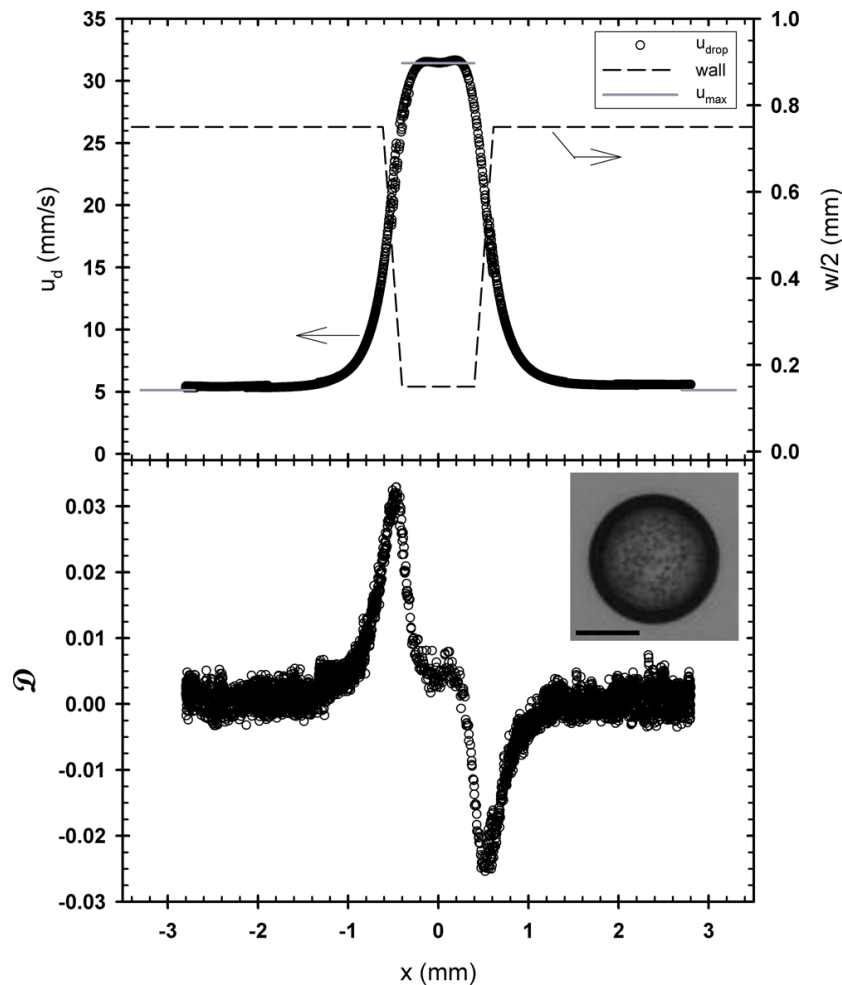


Figure 3. Droplet velocity and deformation through a constriction. Total flow $q_{\text{tot}} = 4.81 \text{ mL h}^{-1}$; $a_0 = 29 \mu\text{m}$; confinement $2a/h = 0.19$; $w = 1500 \mu\text{m}$; $w_c = 300 \mu\text{m}$; $h = 278 \pm 18 \mu\text{m}$. Inset image shows a droplet with particle tracers, scale bar represents $50 \mu\text{m}$. Droplet velocity matches the predicted centerline velocity u_{max} for a rectangular channel. The standard uncertainty of u_d and \mathcal{D} are $\pm 0.091 \text{ mm s}^{-1}$ and ± 0.0047 , respectively.

mobility of the interface, a property of at least as much interest as the tension itself. In the wide portion of the channel, a relatively slow and simple fountain flow occurs inside the drop. The flow inside the drop is faster and more complex when it passes the constriction, and some internal mixing takes place which further facilitates mass transfer. As the drop approaches or exits the constriction (i.e. when the extension rate is relatively high), four vortices in the drop are observed, and as expected the extension of the fluid inside the drop is transverse to the stretching direction outside. In later sections, we report the circulation velocity measured as the forward velocity at the center of the drop and only in the wide portion of the channel far from constrictions.

From the aforementioned measurements, e.g. time-dependant interfacial tension, we can evaluate various parameters noted in section 2 and estimate the dominant mechanism

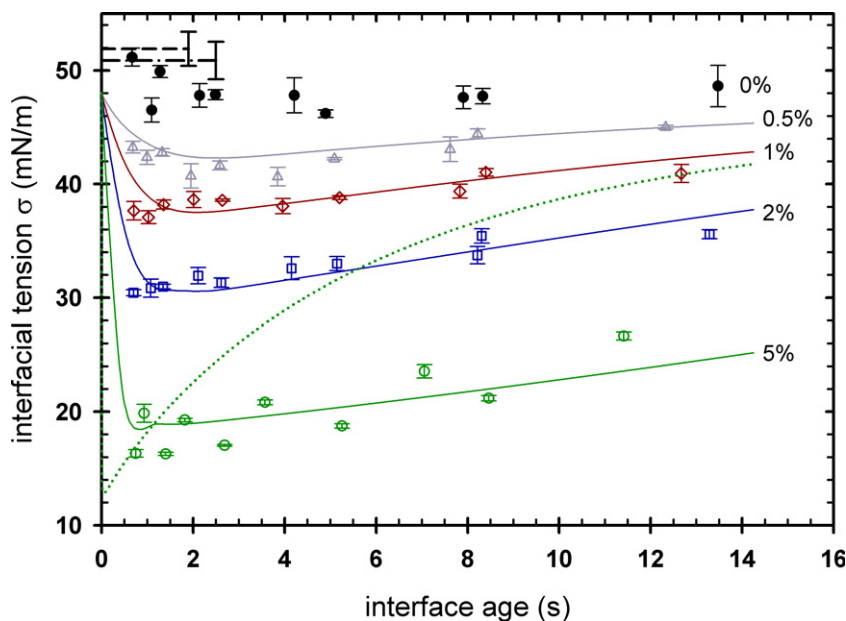


Figure 4. Interfacial tension as a function of interface age for various initial butanol concentrations for water in mineral oil. Butanol-free systems are shown as dash-dotted line from current microfluidic setup with no tracer particles, and dashed line from pendant drop. Solid lines represent model predictions from a mixed diffusion-kinetic model. The dotted line represents a diffusion-controlled model for 5% mass fraction butanol with the appropriate surfactant equilibrium distribution applied to the interface.

for surfactant mass transfer. The internal Peclet number ranges in our experiments from approximately 1 to 20 in the channel and 20 to 100 in the constrictions. As a consequence, convective transport inside the drop is significant, and we anticipate that the drop is effectively well mixed. Diffusion outside the drop across streamlines occurs in approximately $a^2/D = [0.5, 3]$ s. As mentioned previously, R_{D-K} (equation (1)) is predicted to be approximately $[80, 200]$ μm , depending on butanol concentration. Therefore, mass transport of butanol is expected to be governed by kinetic interfacial transport and mixed kinetic-diffusion transport. The question of the limiting mass transfer process in these microchannel flows will be explored more quantitatively in later sections. In addition, the influence of interfacial concentration on interfacial mobility will also be addressed.

4.2. Interfacial tension versus drop age

Following the procedure outlined in section 3.6, the interfacial tension is measured at various constrictions (interface ages) along the channel. Because of the nature of our microfluidic system, we have the advantage of performing a large number of measurements in a relatively short time. The interfacial tension values listed in figure 4 are averages of at least five measurements (error bars are one standard deviation), with the typical uncertainty in a single measurement (fit to Taylor analysis, equation (7)) being approximately $0.5\text{--}3$ mN m^{-1} . The interfacial tension depends weakly on interface age (figure 4), and the tension increases modestly with increasing interface age, at a rate of nearly 1 $\text{mN m}^{-1} \text{ s}^{-1}$ for

higher concentrations of butanol (2 and 5% mass fraction). The concentration continuously decreases as the butanol transfers to the oil and is dispersed. The drop size a_0 was varied by a factor of about 1.7 with surprisingly little effect on the interfacial tension. This size-independence is a signature of kinetically limited transfer (equation (5)). In the kinetic limit, the rate of decrease of the interfacial concentration is independent of a . A weak effect of a remains, since the maximum value of Γ during the mass transfer process depends on a and c_0 . In contrast, the diffusion time depends strongly on a , i.e. a^2/D . The dotted and solid lines in figure 4 are the predictions from finite-element modeling, and will be described in more detail in a later section.

We note that the dispersion of butanol here is unlike a Taylor–Aris dispersion (Aris 1956, Taylor 1953), since the experimental time is not sufficiently long for the solute to fully sample the channel cross section. Moreover, when the solute reaches the wall it is not reflected or contained in the channel. Instead it may escape as it diffuses into and through the PDMS.

After complete extraction of butanol from the water to the surrounding oil (and elastomer PDMS device body) at times much longer than studied here, the interfacial tension of pure mineral oil and water is expected. If the channels were instead impenetrable to butanol, then the long time limit would be set by the dilution limit. Since the drop is relatively small (a approximately $0.1h$), this limit itself represents an exceedingly small concentration of butanol. As will be shown in section 4.4, the equilibrium distribution coefficient between the phases is not unity. Considering this factor, the dilution limit is approximately two orders of magnitude less than the starting butanol concentration.

4.3. Drop circulation

For most of the interfacial tension measurements in figure 4, i.e. when particle tracers were present, the internal drop circulation was measured at the drop center and plotted in figure 5 (the circulation velocity \hat{u} is plotted versus the interfacial tension so that the plot would be model-independent). A value of $\hat{u} = 0.5$ is expected for mobile interfaces (Nadim and Stone 1991). Significant interfacial retardation was seen, however, with a rough trend of stronger retardation occurring at low surfactant concentration (higher tension). At higher surfactant concentration, the surfactant exchange is more rapid, therefore the interfacial motion is much greater and approaches the limit of full mobility, i.e. $\hat{u} = 0.5$. This effect is termed remobilization (Stebe and Maldarelli 1994, Stebe *et al* 1991).

When no butanol is added, we expect data on this plot at $\sigma = 52 \text{ mN m}^{-1}$ and $\hat{u} = 0.5$. Surprisingly, however, the retardation is substantial, and σ measured without butanol and with particle tracers is approximately $48 \pm 2 \text{ mN m}^{-1}$, measurably less than without tracers. These two results, interfacial tension reduction and interfacial retardation, indicate that the interface is contaminated with either the particles or an accompanying surface-active impurity. However, we have observed that the particles do not go to the interface, thus implicating an impurity, perhaps a residue from the particle synthesis. Pendant drop tensiometry also indicates the presence of this impurity. For the particle tracer solution, a substantial reduction in σ was observed by the pendant drop method, decreasing from 52 to approximately 40 mN m^{-1} , during a period of 30 min. In contrast, with pure water drops, σ is much more stable, decreasing only slightly to approximately 51.1 mN m^{-1} in the same period.

These results indicate that some surface-active impurity is present in the particle suspension, and it is this surface-active component that immobilizes the interface. However,

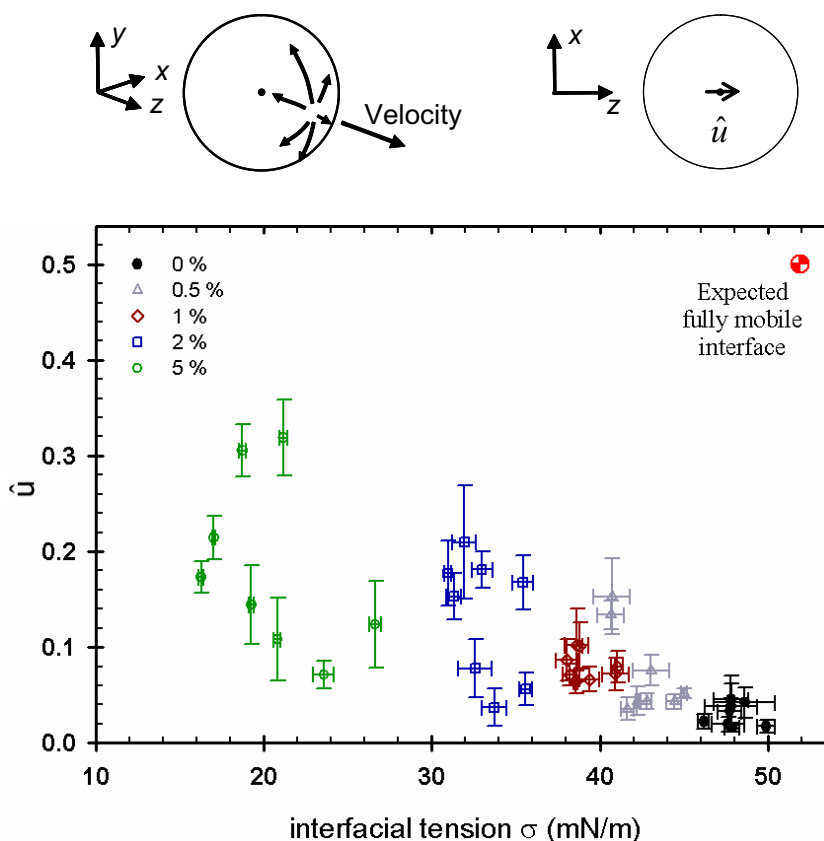


Figure 5. Internal circulation velocity \hat{u} versus interfacial tension. Note at high tension the interface is immobilized. At low interfacial tension, where surfactant exchange is more rapid, the interface is partially remobilized. Schematics of the interfacial flow (left) and internal circulation \hat{u} (right) are shown.

when a large concentration of butanol is present, interfacial tension gradients are dominated by the distribution of butanol and not the surface active impurity, since Marangoni effects arise from gradients in interfacial tension not in interfacial concentration directly.

In spite of the severe retardation, the interface velocity remains significant: the internal Peclet number is still substantial (Pe_{int} is approximately 1–20). Therefore, convection in the drop, and the type of convection, i.e. a fountain flow, remains effective in bringing solute from the center of the drop to near the interface, even in the most severely retarded cases.

4.4. Pendant drop tensiometry and equilibrium interfacial tension

To analyze the microfluidic data in terms of a kinetic model, it is helpful to measure the ratio of desorption to adsorption coefficients in both phases independently. Therefore, pendant drop tensiometry was used to measure the interfacial tension as a function of surfactant concentration in either the aqueous or oil phases (figure 6). We thereby demonstrate the suitability of the Langmuir model and measure the equilibrium distribution coefficient of butanol between the two phases. In this study, water drops in oil media were investigated, and butanol was added to either the water or oil phases. Because of the unequal partitioning of the butanol across the

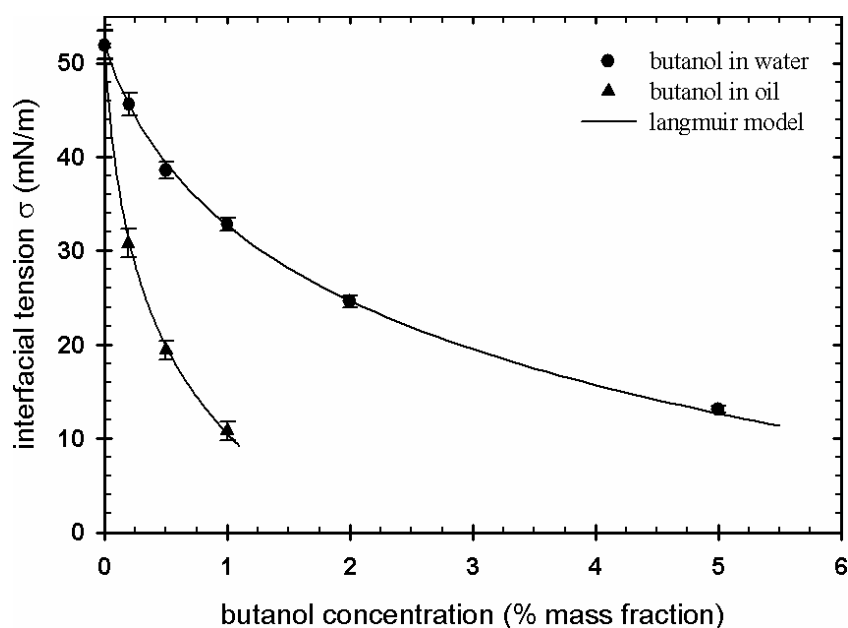


Figure 6. Equilibrium interfacial tension between water and heavy mineral oil as a function of butanol concentration in the water. Symbols represent data from the pendant drop method and the curves are fits according to the Langmuir model.

interface, care must be taken when analyzing pendant drop data from our system; therefore, we will describe the procedure in detail.

The data obtained is similar to that of Ferrari *et al* (1997) and Liggieri *et al* (1997). Specifically, we find that when the butanol is in the water drop initially, the tension rapidly (<30 s) decreases to a minimum and then slowly (several hours to days) increases. At the minimum, butanol has transferred across the interface and infused the oil adjacent to the interface at a concentration in equilibrium with the interface. Eventually the butanol diffuses in the oil over much longer distances, causing its overall concentration to decline and the interfacial tension to slowly rise. The value of this minimum tension is taken to be the equilibrium tension at the given concentration, since it occurs long before dilution. A major reason that the dilution is so slow is that the local equilibrium concentration of butanol in oil adjacent to the interface is substantially less than that in water, as determined below, and thus reducing concentration gradients markedly (Liggieri *et al* 1997). When the butanol is added to the oil phase, the tension decreases slowly (within 1 min to a couple of hours, depending on concentration) to an asymptote, which is taken to be the equilibrium tension since the concentration remains at nearly the initial value due to the fact that the relative volume of the oil is a few hundred times that of the water. At these quasi-equilibrium conditions, the concentrations of butanol adjacent to the interface are steady. The longer equilibration time observed when butanol is added to the oil phase is again a result of the unequal partitioning of the butanol across the interface. This partitioning is evident from the isotherms generated (figure 6), which demonstrates that at local equilibrium (equal tension), the concentration of butanol adjacent to the interface is substantially (approximately six times) lower in the oil phase, in comparison to that in the water phase.

According to the Langmuir model, the interfacial tension is given by the following expression:

$$\begin{aligned}\sigma &= \sigma_0 - kT \Gamma_{\max} \ln(1 + c_w/c_w^*) \\ &= \sigma_0 - kT \Gamma_{\max} \ln(1 + c_{\text{oil}}/c_{\text{oil}}^*) \\ &= \sigma_0 + kT \Gamma_{\max} \ln(1 - \Gamma/\Gamma_{\max}),\end{aligned}\quad (13)$$

where k is the Boltzmann constant and T is the temperature. This model approximates the data of figure 6 (indicating suitability of the Langmuir model) when $\Gamma_{\max} = 6 \times 10^{-6} \text{ mol m}^{-2}$, $c_w^* = 50 \text{ mol m}^{-3}$ (0.37% mass fraction), and $c_{\text{oil}}^* = 8.6 \text{ mol m}^{-3}$ (0.063% mass fraction). These same values (Γ_{\max} and c_w^*) were already found to apply to the effect of butanol on the tension of the air water interface (Joos and Serrien 1989). The interfacial structures at the two different interfaces (oil–water and air–water) are therefore similar, consistent with their comparable interfacial pressures. As noted above, the ratio $K = c_w^*/c_{\text{oil}}^*$ is the equilibrium distribution coefficient, equal to approximately 5.8. Although $c_i^* = \alpha_i/\beta_i$ may be determined by pendant drop tensiometry, the kinetic coefficients α_i and β_i themselves are often, and in this case, inaccessible by pendant drop tensiometry. Therefore, in the subsequent section, the data of figure 4 will be analyzed in reference to that of figure 6 to evaluate the kinetic coefficients α_i for desorption.

4.5. Applying the mixed kinetic model and comparing to experimental data

Since both the interfacial tension and the drop circulation have been determined, we can now discuss the relevance of the various surfactant mass transfer parameters on the interfacial dynamics. First, a comparison between models will be made, and then comparisons to experimental data will be performed.

Concentration-time profiles for the mixed kinetic-diffusion model are calculated by finite-element modeling, and shown in figure 7 along with a diffusion-limited case (equation (3)) and a case where convection (internal mixing) is considered. The following parameters were used for these calculations. As noted above, the diffusivity in each phase was assumed to be $D = 9.5 \times 10^{-10} \text{ m}^2 \text{ s}^{-1}$, and the drop radius was chosen from a typical experimental value, viz. $a = 43 \mu\text{m}$. $\Gamma_{\max} = 6 \times 10^{-6} \text{ mol m}^{-2}$ was determined from pendant drop measurements. The distribution coefficient K was taken to be either 1 (no partitioning) or 5.8, to illustrate the effect of surfactant partitioning across the interface. Concerning the magnitude of the kinetic coefficients, $\alpha_{\text{oil}} = \alpha_w$ were either $1 \times 10^4 \text{ s}^{-1}$ or 70 s^{-1} to illustrate, respectively, the diffusion limit or mixed kinetic transfer. Solid lines in figure 7 represent butanol concentrations in the droplet center, and dashed lines represent the concentration adjacent to the interface.

The various cases illustrated in figure 7 differ both qualitatively and quantitatively. The mixed kinetic model is more than an order of magnitude slower than the diffusion limited model (curve a versus d, respectively). The diffusion model of equation (3) (curve d) assumes no partitioning across the interface (i.e. $K = 1$); however, such partitioning has an influence on the diffusion limited transport (b) (Liggieri *et al* 1997). For example, if the surfactant is partitioned to the source, the transfer is slower than if it is partitioned to the destination. Two diffusion limited cases ($\alpha_{\text{oil}} = \alpha_w = 1 \times 10^4 \text{ s}^{-1}$) with and without partitioning are plotted in figure 7 (curves b and c, respectively), and the non-partitioned case ($K = 1$) agrees well with equation (3) (curve d), as expected. The large differences caused by partitioning in the diffusion-limited cases are less evident in the mixed kinetic-diffusion case, likely due to the limiting

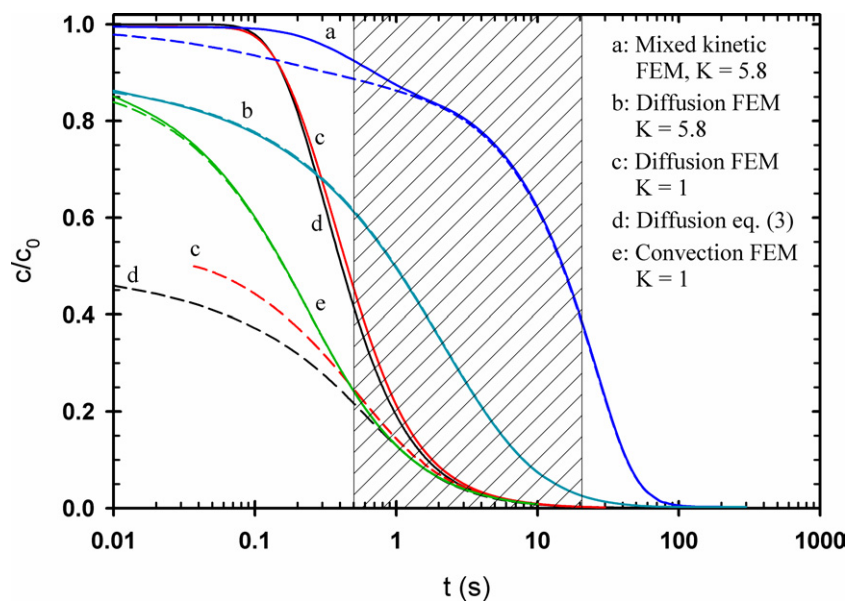


Figure 7. Comparison of the mixed kinetic model, and diffusion and convection limits without surfactant partitioning for $a = 43 \mu\text{m}$, $c_0/c^* = 10$ and $D = 9.5 \times 10^{-10} \text{m}^2 \text{s}^{-1}$. Solid and dashed lines indicate butanol concentration at the droplet center and adjacent to the interface, respectively. The experimental window with the current setup is highlighted.

kinetics at the interface (not shown). To simulate the effect of convective mixing in the drop, the diffusivity there can be increased artificially. This case is plotted as curve e in figure 7 ($K = 1$; $\alpha_{\text{oil}} = \alpha_{\text{w}} = 1 \times 10^4 \text{s}^{-1}$; and diffusivity in the drop increased by a factor of 100). In such a case, the concentration in the drop is essentially uniform and the solid and dashed lines merge together and follow an intermediate curve. When the transport across the interface is slowed by adsorption/desorption kinetics, a similar effect occurs. The bump in the mixed kinetic model (a) occurring between 0.1 and 1 s is due to a relatively rapid equalization of surfactant concentration in the drop. Internal convection simply causes this equalization at earlier times.

For comparison with experimental data, interfacial tension values predicted by the mixed kinetic-diffusion model with $K = 5.8$ are shown as solid lines in figure 4. Average values of the experimental drop size a_0 were used in the model for each concentration. We note that because α_{oil} and α_{w} are both fitting parameters in the mixed kinetic-diffusion model, a wide parameter space exists in which to conduct fitting to the data in figure 4. α_{oil} and α_{w} were both individually and systematically varied, with the best fit to all datasets occurring at $\alpha_{\text{oil}} = \alpha_{\text{w}} = 70 \text{s}^{-1}$. Both the minimum and slope of the curves in figure 4 can be changed by varying the desorption coefficients: they have similar effect on the slope (large α_i increase the slope) and compensating effect on the minimum (larger α_{w} lowers the minimum, while larger α_{oil} raises it). We estimate the uncertainty on α_{oil} and α_{w} to be approximately $\pm 50 \text{s}^{-1}$: multiplying or dividing values of α_{oil} and α_{w} by $\sqrt{2}$ does not significantly change the quality of the fit in figure 4; however, multiplying or dividing $\alpha_{\text{oil}} = \alpha_{\text{w}}$ by a factor of 2 produces poor quality fits.

The mixed kinetic-diffusion model is in good agreement with the experimental data at all but very short times, verifying that our system indeed follows the mixed kinetic-diffusion model. The disagreement at very short times likely comes from neglecting convective effects

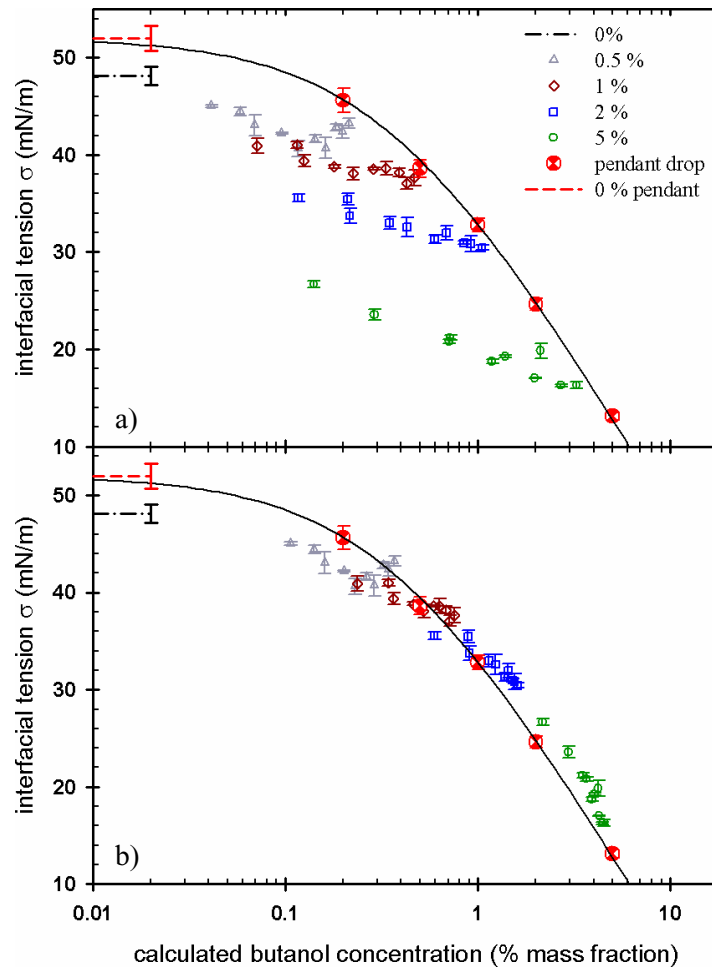


Figure 8. Interfacial tension as a function of butanol concentration for water in mineral oil: (a) for the diffusion limited case with surfactant partitioning ($\alpha_w = \alpha_{oil} = 1 \times 10^4 \text{ s}^{-1}$, $K = 5.8$), and (b) taking into account adsorption/desorption kinetics ($\alpha_w = \alpha_{oil} = 70 \text{ s}^{-1}$, $K = 5.8$). Hourglass symbols represent steady-state pendant drop data, and the solid line represents a fit to the Langmuir model (equation (5) and figure 6).

that the drop experiences in the interval between the T-junction and the first measurement point. For comparison, the interfacial tension predicted by the partitioned diffusion-controlled model ($K = 5.8$; curve b in figure 7) is shown as a dotted line in figure 4 for 5% mass fraction of butanol. Interfacial kinetics are greatly accelerated in this model and thus mass transfer occurs more quickly and the interfacial tension is overpredicted at all but very short times, where it is underpredicted. Clearly, interfacial kinetics must be considered.

The diffusion and mixed kinetic models can be compared further by using them with the interfacial tension data of figure 4 to generate adsorption isotherms (figure 8). To construct the isotherms, concentration-time profiles were calculated by the finite-element models, and butanol concentrations were calculated corresponding to the times at which interfacial tension measurements were performed in the microfluidic device. The mixed kinetic-diffusion model produces a superior collapse of the data, and the fitting parameters are the desorption coefficients

α_w and α_{oil} , determined from figure 4. Consistency with the microfluidic data depends significantly on the desorption coefficients. These coefficients, moreover, have an even more fundamental effect on the shape of the plot, so that even in the absence of reference data from pendant drop (which was used to determine the surfactant equilibrium distribution coefficients), the desorption coefficients could be determined, leading to an independent method to determine the adsorption isotherm. The deviations at low concentration in figure 8(b) can be explained by the presence of the surface-active impurity perceived in section 4.3, whereas deviations at high concentration may be due to the loss of butanol through diffusion into the PDMS in the input channel or dilution from shear dispersion (section 2.2), which were not accounted for.

To summarize, the kinetic constants for adsorption and desorption of butanol in a water/mineral oil system were determined through the use of a microfluidic approach combined with simple modeling. Langmuir kinetics were assumed at the interface, and the importance of surfactant partitioning was demonstrated.

5. Conclusions and future directions

These experiments demonstrate that interfacial tension, surfactant mass transfer and interfacial retardation can be measured in a single experiment, so that interfacial properties and mobility can be correlated directly. At low concentration of butanol the interfacial tension is not reduced much, but the interfacial mobility is severely retarded. However, the interface is remobilized at higher surfactant concentration. The interfacial tension is described well by Langmuir kinetics and the parameters for interfaces with mineral oil (studied here) are similar to those previously found at air interfaces. The mass transfer of butanol from water drops into the surrounding flowing oil was shown to be well described by a mixed kinetic-diffusion limited model, and the desorption rate coefficient (from the interface to the oil) is measured to be approximately 70 s^{-1} .

The microfluidic approach employed here facilitates measurements of the interrelated quantities of interfacial tension, surfactant mass transfer kinetics and Marangoni effects in a single experiment utilizing two-phase flows under conditions, particularly droplet size, that are relevant to industrial and microfluidic applications. At this reduced droplet length scale, the shift from diffusion-controlled to mixed kinetic-diffusion mass transfer was verified, stressing the importance of measurement at reduced length scales relating to processing applications. These measurements along with measurements of Marangoni effects (interfacial immobilization) are essential in understanding the dynamics of two-phase systems, i.e. emulsions, and moving toward the ultimate goal of accurately predicting emulsion performance and stability.

Acknowledgment

JDM gratefully acknowledges financial support through a National Research Council—NIST postdoctoral fellowship.

Appendix

In general, droplets entering a constriction experience a mixture of shear and extensional flows, with the relative strength of each type of flow determined by many factors including the channel geometry, drop size, drop height and confinement. To simplify, we consider aspect ratios such

Table A.1. The ratio of extension to shear $\dot{\epsilon}_1^2/(\dot{\gamma}^2/2)$ through a constriction ($w_x = w \rightarrow w_c$) for varying channel geometry and droplet height. Aspect ratio is h/w , and aspect ratios listed below are typical limits for our experimental set-up.

Aspect ratio h/w	y'		
	0.1	0.3	0.45
0.067	0.6 \rightarrow 20	0.03 \rightarrow 0.8	0.001 \rightarrow 0.03
0.183	5 \rightarrow 100	0.2 \rightarrow 6	0.009 \rightarrow 0.2
0.3	10 \rightarrow 300	0.6 \rightarrow 20	0.02 \rightarrow 0.6

that $w, w_c \gg h$, so that the velocity scales inversely with the channel cross section, where w and w_c are the channel and constriction widths, respectively. Thus, the velocity in the constriction is

$$u = u_0(1 - 4y'^2) \frac{w}{w_x}, \quad (\text{A.1})$$

where u_0 is the undisturbed centerline velocity, w_x is the channel width as a function of x as the width changes from w to w_c in the constriction (over a length of ℓ), and y' is the dimensionless drop height given by equation (6). Let us consider three cases: (i) the droplet essentially on the centerline, (ii) the droplet near the centerline, and (iii) the droplet near the wall. The rate of strain tensor for a fluid element at $z = 0$ is in general

$$\underline{\underline{D}} = \frac{1}{2}(\nabla u + \nabla u^T) = \begin{bmatrix} \dot{\epsilon} & \dot{\gamma}/2 & 0 \\ \dot{\gamma}/2 & 0 & 0 \\ 0 & 0 & -\dot{\epsilon} \end{bmatrix}. \quad (\text{A.2})$$

Case (1): if the droplet is essentially on the centerline, the extension rate is given by

$$\dot{\epsilon}_1 = \frac{du}{dx} = u_0(1 - 4y'^2) \frac{w}{w_x^2} \frac{w - w_c}{\ell} = -\dot{\epsilon}_2, \quad (\text{A.3})$$

and the shear rate is essentially zero $\dot{\gamma} \approx 0$. In this case, extension dominates.

Case (2): with the droplet near the centerline, the extension rate is given by equation (A.3) and the shear rate is

$$\dot{\gamma} = \frac{du}{dy} = -8y' \frac{u_0}{h} \frac{w}{w_x}. \quad (\text{A.4})$$

Under these circumstances, the principal deformation rate is $\sqrt{\dot{\epsilon}_1^2 + \dot{\gamma}^2/2}$. Table A.1 enumerates the ratio $\dot{\epsilon}_1^2/(\dot{\gamma}^2/2)$ for a variety of conditions of channel aspect ratio and drop height y' . For each entry the two numbers illustrate the range of values of this ratio obtained by varying w_x between w and w_c . For large aspect ratio (e.g. $h/w = 0.3$), the ratio of extension to shear is large and the flow is essentially planar extension. Aspect ratios given here represent approximate practical upper and lower limits for our devices.

Case (3): for the droplet approaching the wall ($y' = \pm 0.3$), the ratio $\dot{\epsilon}_1^2/(\dot{\gamma}^2/2)$ entering the constriction increases from $O(0.01)$ to $O(1)$ and $O(1)$ to $O(10)$ for small and large aspect ratios, respectively. This case is shear dominated at small aspect ratios. If $y' = \pm 0.45$, the extension to shear ratio increases from $O(0.001)$ to $O(0.01)$ and $O(0.01)$ to $O(1)$ for small and large aspect ratios, respectively (again, see table A.1). However, we have found

that we are only able to operate within the limits $-0.3 < y' < 0.3$ (at confinement $2a/h \approx 0.3$) in our devices. Of course, this limitation is expected to be dependent on drop size (confinement) and is most likely due to finite drop size and wall migration (Chan and Leal 1979, Hudson 2003).

From the above analysis, it is clear that the flow complexity can be easily tuned by varying the channel geometry and droplet height, while keeping confinement relatively small.

References

- Ahmed B, Barrow D and Wirth T 2006 Enhancement of reaction rates by segmented fluid flow in capillary scale reactors *Adv. Synth. Catal.* **348** 1043–8
- Alvarez N J, Walker L M and Anna S L 2009 private communication
- Anna S L, Bontoux N and Stone H A 2003 Formation of dispersions using ‘flow focusing’ in microchannels *Appl. Phys. Lett.* **82** 364–6
- Aris R 1956 On the dispersion of a solute in a fluid flowing through a tube *Proc. R. Soc. A* **235** 67–77
- Baroud C N, Okkels F, Menetrier L and Tabeling P 2003 Reaction–diffusion dynamics: Confrontation between theory and experiment in a microfluidic reactor *Phys. Rev. E* **67** 060104
- Benninger R K P, Hofmann O, Onfelt B, Munro I, Dunsby C, Davis D M, Neil M A A, French P M W and de Mello A J 2007 Fluorescence-lifetime imaging of DNA-dye interactions within continuous-flow microfluidic systems *Angew. Chem. Int. Ed. Engl.* **46** 2228–31
- Berthier J, Tran V M, Mittler F and Sarrut N 2009 The physics of a coflow micro-extractor: Interface stability and optimal extraction length *Sensors Actuators A* **149** 56–64
- Bryden M D and Brenner H 1999 Mass-transfer enhancement via chaotic laminar flow within a droplet *J. Fluid Mech.* **379** 319–31
- Burns J R and Ramshaw C 2001 The intensification of rapid reactions in multiphase systems using slug flow in capillaries *Lab Chip* **1** 10–5
- Cabral J T and Hudson S D 2006 Microfluidic approach for rapid multicomponent interfacial tensiometry *Lab Chip* **6** 427–36
- Carslaw H S and Jaeger J C 1959 *Conduction of Heat in Solids* (Oxford: Clarendon)
- Chan P C H and Leal L G 1979 Motion of a deformable drop in a 2nd-order fluid *J. Fluid Mech.* **92** 131–70
- Chatwin P C and Sullivan P J 1982 The effect of aspect ratio on longitudinal diffusivity in rectangular channels *J. Fluid Mech.* **120** 347–58
- Dessimoz A L, Cavin L, Renken A and Kiwi-Minsker L 2008 Liquid–liquid two-phase flow patterns and mass transfer characteristics in rectangular glass microreactors *Chem. Eng. Sci.* **63** 4035–44
- Duffy D C, McDonald J C, Schueller O J A and Whitesides G M 1998 Rapid prototyping of microfluidic systems in poly(dimethylsiloxane) *Anal. Chem.* **70** 4974–84
- Edel J B, Fortt R, deMello J C and deMello A J 2002 Microfluidic routes to the controlled production of nanoparticles *Chem. Commun.* (10) 1136–7
- Fainerman V B and Miller R 1995 Dynamic surface-tension measurements in the submillisecond range *J. Colloid Interface Sci.* **175** 118–21
- Fainerman V B, Kazakov V N, Lylyk S, Makievski A V and Miller R 2004 Dynamic surface tension measurements of surfactant solutions using the maximum bubble pressure method—limits of applicability *Colloids Surf. A* **250** 97–102
- Fainerman V B, Mys V D, Makievski A V, Petkov J T and Miller R 2006 Dynamic surface tension of micellar solutions in the millisecond and submillisecond time range *J. Colloid Interface Sci.* **302** 40–6
- Ferrari M, Liggieri L, Ravera F, Amodio C and Miller R 1997 Adsorption kinetics of alkylphosphine oxides at water/hexane interface. 1. Pendant drop experiments *J. Colloid Interface Sci.* **186** 40–5

- Gonzalez-Mancera A 2007 Effects of non-linear interfacial mechanics on the transient response of a drop to an external flow field *Mechanical Engineering* (College Park, MD: University of Maryland)
- Grigoriev R O 2005 Chaotic mixing in thermocapillary-driven microdroplets *Phys. Fluids* **17** 033601
- Grigoriev R O, Schatz M F and Sharma V 2006 Chaotic mixing in microdroplets *Lab Chip* **6** 1369–72
- He M Y, Edgar J S, Jeffries G D M, Lorenz R M, Shelby J P and Chiu D T 2005 Selective encapsulation of single cells and subcellular organelles into picoliter- and femtoliter-volume droplets *Anal. Chem.* **77** 1539–44
- Hetsroni G and Haber S 1970 The flow in and around a droplet or bubble submerged in an unbound arbitrary velocity field *Rheol. Acta* **9** 488–96
- Hiller W and Kowalewski T A 1987 An experimental study of the lateral migration of a droplet in a creeping flow *Exp. Fluids* **5** 43–8
- Hu Y T and Lips A 2003 Estimating surfactant surface coverage and decomposing its effect on drop deformation *Phys. Rev. Lett.* **91** 044501
- Hudson S D 2003 Wall migration and shear-induced diffusion of fluid droplets in emulsions *Phys. Fluids* **15** 1106–13
- Hudson S D, Cabral J T, Goodrum W J Jr, Beers K L and Amis E J 2005 Microfluidic interfacial tensiometry *Appl. Phys. Lett.* **87** 081905
- Jin F, Balasubramaniam R and Stebe K J 2004 Surfactant adsorption to spherical particles: The intrinsic length scale governing the shift from diffusion to kinetic-controlled mass transfer *J. Adhes.* **80** 773–96
- Joos P and Serrien G 1989 Adsorption-kinetics of lower alkanols at the air water interface—effect of structure makers and structure breakers *J. Colloid Interface Sci.* **127** 97–103
- Kamholz A E, Schilling E A and Yager P 2001 Optical measurement of transverse molecular diffusion in a microchannel *Biophys. J.* **80** 1967–72
- Kamholz A E, Weigl B H, Finlayson B A and Yager P 1999 Quantitative analysis of molecular interaction in a microfluidic channel: the T-sensor *Anal. Chem.* **71** 5340–7
- Kamholz A E and Yager P 2001 Theoretical analysis of molecular diffusion in pressure-driven laminar flow in microfluidic channels *Biophys. J.* **80** 155–60
- Kang T, Han J and Lee K S 2008 Concentration gradient generator using a convective-diffusive balance *Lab Chip* **8** 1220–2
- Kim J W, Utada A S, Fernandez-Nieves A, Hu Z B and Weitz D A 2007 Fabrication of monodisperse gel shells and functional microgels in microfluidic devices *Angew. Chem. Int. Ed. Engl.* **46** 1819–22
- Kumemura M and Korenaga T 2006 Quantitative extraction using flowing nano-liter droplet in microfluidic system *Anal. Chim. Acta* **558** 75–9
- Li S F Y and Ong H M 1990 Infinite dilution diffusion-coefficients of several alcohols in water *J. Chem. Eng. Data* **35** 136–7
- Liggieri L, Ravera F, Ferrari M, Passerone A and Miller R 1997 Adsorption kinetics of alkylphosphine oxides at water/hexane interface. 2. Theory of the adsorption with transport across the interface in finite systems *J. Colloid Interface Sci.* **186** 46–52
- Lin S Y, McKeigue K and Maldarelli C 1990 Diffusion-controlled surfactant adsorption studied by pendant drop digitization *AIChE J.* **36** 1785–95
- Lin S Y, Wang W J and Hsu C T 1997 Adsorption kinetics of 1-octanol at the air–water interface *Langmuir* **13** 6211–8
- Mary P, Studer V and Tabeling P 2008 Microfluidic droplet-based liquid-liquid extraction *Anal. Chem.* **80** 2680–7
- Matthews S M, Elder A D, Yunus K, Kaminski C F, Brennan C M and Fisher A C 2007 Quantitative kinetic analysis in a microfluidic device using frequency-domain fluorescence lifetime imaging *Anal. Chem.* **79** 4101–9
- Miller R and Kretzschmar G 1991 Adsorption-kinetics of surfactants at fluid interfaces *Adv. Colloid Interface Sci.* **37** 97–121
- Miller R, Joos P and Fainerman V B 1994 Dynamic surface and interfacial-tensions of surfactant and polymer-solutions *Adv. Colloid Interface Sci.* **49** 249–302
- Milliken W J and Leal L G 1994 The influence of surfactant on the deformation and breakup of a viscous drop—the effect of surfactant solubility *J. Colloid Interface Sci.* **166** 275–85

- Milliken W J, Stone H A and Leal L G 1993 The effect of surfactant on the transient motion of newtonian drops *Phys. Fluids A* **5** 69–79
- Nadim A and Stone H A 1991 The motion of small particles and droplets in quadratic flows *Stud. Appl. Math.* **85** 53–73
- Nie Z H, Xu S Q, Seo M, Lewis P C and Kumacheva E 2005 Polymer particles with various shapes and morphologies produced in continuous microfluidic reactors *J. Am. Chem. Soc.* **127** 8058–63
- Nisisako T, Torii T and Higuchi T 2002 Droplet formation in a microchannel network *Lab Chip* **2** 24–6
- Nisisako T, Torii T, Takahashi T and Takizawa Y 2006 Synthesis of monodisperse bicolored janus particles with electrical anisotropy using a microfluidic co-flow system *Adv. Mater.* **18** 1152
- Pan R N, Green J and Maldarelli C 1998 Theory and experiment on the measurement of kinetic rate constants for surfactant exchange at an air/water interface *J. Colloid Interface Sci.* **205** 213–30
- Passerone A, Liggieri L, Rando N, Ravera F and Ricci E 1991 A new experimental-method for the measurement of the interfacial-tension between immiscible fluids at zero bond number *J. Colloid Interface Sci.* **146** 152–62
- Pawar Y and Stebe K J 1996 Marangoni effects on drop deformation in an extensional flow: the role of surfactant physical chemistry. 1. Insoluble surfactants *Phys. Fluids* **8** 1738–51
- Rallison J M 1984 The deformation of small viscous drops and bubbles in shear flows *Ann. Rev. Fluid Mech.* **16** 45–66
- Ristenpart W D, Wan J D and Stone H A 2008 Enzymatic reactions in microfluidic devices: Michaelis-Menten kinetics *Anal. Chem.* **80** 3270–6
- Salmon J B, Dubroq C, Tabeling P, Charier S, Alcor D, Jullien L and Ferrage F 2005 An approach to extract rate constants from reaction—diffusion dynamics in a microchannel *Anal. Chem.* **77** 3417–24
- Sato K, Hibara A, Tokeshi M, Hisamoto H and Kitamori T 2003 Integration of chemical and biochemical analysis systems into a glass microchip *Anal. Sci.* **19** 15–22
- Shraiman B I 1987 Diffusive transport in a Rayleigh–Benard convection-cell *Phys. Rev. A* **36** 261–7
- Sims C E and Allbritton N L 2007 Analysis of single mammalian cells on-chip *Lab Chip* **7** 423–40
- Stebe K J and Maldarelli C 1994 Remobilizing surfactant retarded fluid particle interfaces. 2. Controlling the surface mobility at interfaces of solutions containing surface-active components *J. Colloid Interface Sci.* **163** 177–89
- Stebe K J, Lin S Y and Maldarelli C 1991 Remobilizing surfactant retarded fluid particle interfaces. 1. Stress-free conditions at the interfaces of micellar solutions of surfactants with fast sorption kinetics *Phys. Fluids A* **3** 3–20
- Stone H A and Leal L G 1990 The effects of surfactants on drop deformation and breakup *J. Fluid Mech.* **220** 161–86
- Stone H A, Nadim A and Strogatz S H 1991 Chaotic streamlines inside drops immersed in steady stokes flows *J. Fluid Mech.* **232** 629–46
- Taylor G I 1932 The viscosity of a fluid containing small drops of another fluid *Proc. R. Soc. A* **138** 41–8
- Taylor G I 1934 The formation of emulsion in definable fields of flow *Proc. R. Soc. A* **146** 501–23
- Taylor G 1953 Dispersion of soluble matter in solvent flowing slowly through a tube *Proc. R. Soc. A* **219** 186–203
- Teh S Y, Lin R, Hung L H and Lee A P 2008 Droplet microfluidics *Lab Chip* **8** 198–220
- Thorsen T, Roberts R W, Arnold F H and Quake S R 2001 Dynamic pattern formation in a vesicle-generating microfluidic device *Phys. Rev. Lett.* **86** 4163–6
- Tokeshi M, Minagawa T, Uchiyama K, Hibara A, Sato K, Hisamoto H and Kitamori T 2002 Continuous-flow chemical processing on a microchip by combining microunit operations and a multiphase flow network *Anal. Chem.* **74** 1565–71
- Utada A S, Lorenceau E, Link D R, Kaplan P D, Stone H A and Weitz D A 2005 Monodisperse double emulsions generated from a microcapillary device *Science* **308** 537–41
- Ward A F H and Tordai L 1946 Time dependence of boundary tensions of solutions. I. The role of diffusion in time effects *J. Chem. Phys.* **14** 453

- Whitesides G M, Ostuni E, Takayama S, Jiang X Y and Ingber D E 2001 Soft lithography in biology and biochemistry *Ann. Rev. Biomed. Eng.* **3** 335–73
- Yeh M C and Chen L J 2001 A modified calibration technique for pendant drop/bubble tensiometry *J. Chin. Inst. Chem. Eng.* **32** 109–16
- Yobas L, Martens S, Ong W L and Ranganathan N 2006 High-performance flow-focusing geometry for spontaneous generation of monodispersed droplets *Lab Chip* **6** 1073–9
- Zhang H, Tumarkin E, Peerani R, Nie Z, Sullan R M A, Walker G C and Kumacheva E 2006 Microfluidic production of biopolymer microcapsules with controlled morphology *J. Am. Chem. Soc.* **128** 12205–10